

Neutron Larmor diffraction with double and single precession arm

A.A. van Well and M.T. Rekveldt

Department of Radiation Science and Technology, Faculty Applied Sciences, Delft University of Technology, 2629JB Delft, The Netherlands

a.a.vanwell@tudelft.nl

Abstract

A review is given of double and single arm Larmor diffraction. With the former a lattice-spacing resolution down to 10^{-6} can be obtained. The latter is a good high-resolution alternative if the sample or sample environment disturbs the magnetic field, e.g. ferromagnetic samples or applied magnetic fields. By choosing the tilt angle of the precession fields the optimum resolution can be set at a scattering angle at choice. The resolution for both single-crystal and polycrystalline samples is discussed in depth and is compared with conventional neutron-diffraction techniques.

1. Introduction

One of the areas of research where high-resolution diffraction is crucial is crystal-structure determination of low-symmetry and/or many-component systems. Then, the overlap of Bragg peaks at higher wave-vector transfers Q , corresponding to the smaller lattice parameters d is the limiting factor is the structure refinement. Another class of diffraction studies only investigates a limited number of Bragg peaks. Here the interest lies in the precise determination of a limited number of lattice parameters and/or the distribution thereof. Examples for accurate determination of lattice parameter can be found in the field of phase transitions with very small changes in the lattice parameters [1], weak magneto-elastic effect [2] or engineering materials such as different types and/or heat treatments of inconel [3]. Precise determination of the lattice-parameter distribution, or shape of the Bragg peak, gives unique information in material science. It can be used to discriminate between crystallite-size distribution and micro-strain effects [4], or to study dislocations in composite materials [5].

The latter class of studies is the subject of this paper. The use of Larmor precession of polarized neutrons offers a tool to label the energy transfer or the scattering angle with very high precision. The first application was the spin-echo technique to perform high resolution quasi-elastic neutron scattering introduced by Mezei [6]. The Larmor coding of scattering angle was proposed by Pynn [7], and later applied in small-angle scattering [8] and reflectometry [9]. The application in diffraction, with lattice-parameter resolution of $\Delta d/d \approx 10^{-6}$, the so-called double-arm Larmor diffraction was introduced in [10]. This technique cannot be applied for magnetic samples. Then, an alternative is the one-arm Larmor diffraction technique [11] with a resolution in between the double-arm Larmor diffraction and the conventional, monochromatic or time-of-flight, diffractometers. The subject of this paper is the comparison of these four techniques. In Section 2 the performance of the monochromatic and time-of-flight diffractometer is discussed. In Section 3 the double-arm Larmor diffraction method



is introduced. In Section 4 the single-arm version is treated, with emphasis on the high-resolution focusing condition, and the difference in resolution for mosaic crystalline and poly-crystalline samples. Section 5 discusses the comparison of the different techniques, and the potential application of both Larmor methods.

2. Conventional diffractometers

The vast majority of the present neutron diffractometers can be divided in two types: the monochromatic diffractometer, generally located at continuous neutron sources and the time-of-flight diffractometers, most often used at pulsed sources.

2.1. Monochromatic diffractometers

This mean components of this type of diffractometers are the monochromator characterized by the lattice spacing d_M and mosaic spread β , set at a Bragg angle θ_M , selecting the wavelength λ , the sample position, and an area of detectors covering a range of scattering angles 2θ . The beam divergences between source and monochromator, monochromator and sample, sample and detector are characterized by α_1 , α_2 , and α_3 , respectively. The angular resolution, full width half maximum, $\Delta(2\theta)$ of the diffractometer is given by

$$\Delta(2\theta) = \sqrt{U \tan^2 \theta + V \tan \theta + W}, \quad (1)$$

where U , V and W are functions of α_1 , α_2 , α_3 , β and θ_M [12,13]. The minimum value of $\Delta(2\theta)$ is $\Delta(2\theta)_{\min} = \sqrt{W - V^2/4U}$ for $\tan \theta = -V/2U \approx \tan \theta_M$. The lattice-spacing resolution is through the Bragg relation given by

$$\frac{\Delta d}{d} = \cot \theta \Delta \theta. \quad (2)$$

In Fig. 1(a) the angular resolution for a number of state-of-the-art monochromatic diffractometers is displayed. The corresponding resolution in lattice spacing is shown in Fig. 1(b). Note that the best resolution $\Delta d/d \approx 10^{-3}$ is only reached in a limited d -range.

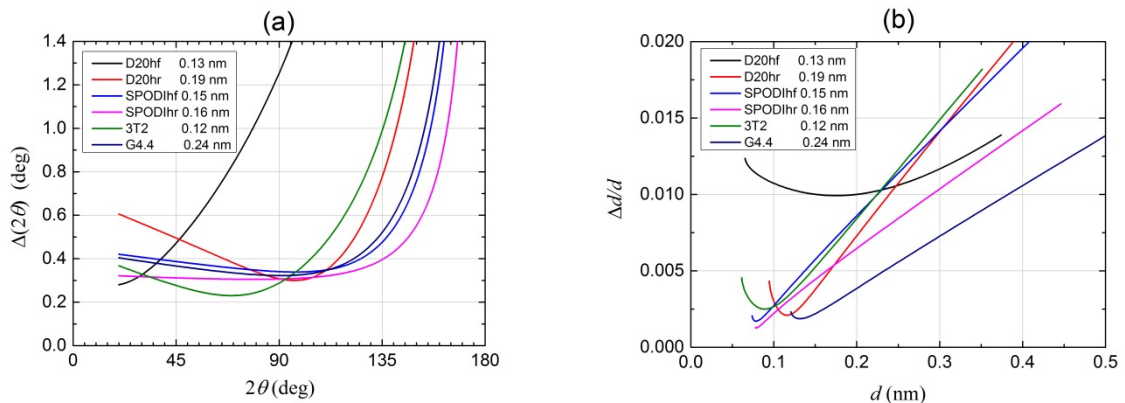


Figure 1. (a) Angular resolution as a function of scattering angle of some monochromatic diffractometers with (b) corresponding resolution in lattice parameter. D20hf and D20hr are a high-flux, Cu (200), and high-resolution, Ge (711) setting of D20, ILL, Grenoble [14], SPODIhf and SPODIhr are a high-flux and high-resolution setting of SPODI, FRM2, Munich [15], 3T3 and G4.4 are diffractometers at LLB [16], Saclay.

2.2. Time-of-flight diffractometers

This type of diffractometers is used at pulsed sources. Essentially the instrument consists of a primary flight path from source to sample, a secondary flight path from sample to detector and an array of detectors covering a large range of scattering angles $2\theta_B$. The resolution is given by [17]

$$\left(\frac{\Delta d}{d}\right)^2 = \left(\frac{\Delta t}{t}\right)_{\text{mod}}^2 + \left(\frac{\Delta L}{L}\right)^2 + \frac{\cot^2 \theta_B}{4} (\Delta \theta^2 + \Delta \phi^2), \quad (3)$$

where Δt is the pulse width of the source, t the time of flight from the source to the detector, L the distance from source to detector, with ΔL its uncertainty, $\Delta \theta$ and $\Delta \phi$ the beam divergences of the incoming and scattered beam, respectively. In Fig. 2 the resolution of the high resolution diffractometer HRPD [18] and the engineering materials diffractometer Engin-x [19], both at ISIS, UK, are shown. In contrast with the monochromatic instruments a large range of lattice parameters is covered at one scattering angle as a result of polychromatic nature of the technique.

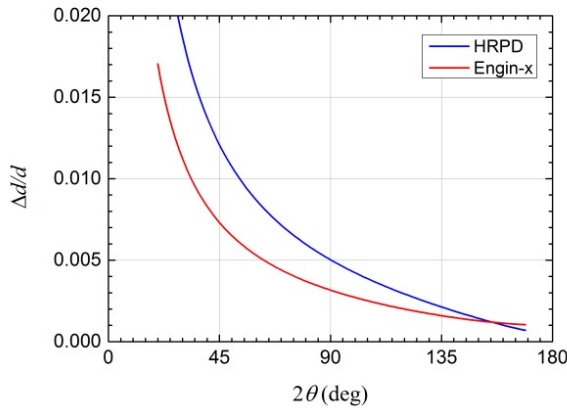


Figure 2. Lattice-spacing resolution of the time-of-flight diffractometer HRPD, [18] and Engin-x [19], ISIS, UK.

HRPD: $\sqrt{\Delta \theta^2 + \Delta \phi^2} = 10 \text{ mrad}$, $\Delta t/t = 5 \cdot 10^{-4}$ (the best time-resolution value, i.e. for $\lambda = 0.1 \text{ nm}$). Engin-x $\sqrt{\Delta \theta^2 + \Delta \phi^2} = 6 \text{ mrad}$, $\Delta t/t = 1 \cdot 10^{-3}$ (valid for $\lambda = 0.2 \text{ nm}$).

3. Double-arm Larmor diffraction

The double-arm Larmor diffraction setup, for the first time described by Rekveldt *et al.* [10], is schematically shown in Fig. 3. The main parts are two well-defined Larmor precession regions with the same, tuneable magnetic field B , one placed in the incoming polarized neutron beam and one in the scattered beam. Before entering the detector that is placed at a scattering angle $2\theta_0$ the polarization of the beam is analyzed by a second polarizer. Here we only describe the geometry with parallel magnetic fields. The anti-parallel, or spin-echo, geometry is described in the Appendix. We first consider the sample to be a *single crystal* with lattice planes parallel to the faces of the precession fields, i.e. $\alpha = 0$ in Fig.3. Then $\mathbf{Q} = \mathbf{G}_{hkl}$. The precession angle in the first and second arm is given by

$$\varphi_1 = \omega_L \frac{L}{v_{1\perp}} = \frac{\omega_L m L}{\hbar} \frac{1}{k_{1\perp}} = 2\pi c B L \frac{1}{k_{1\perp}} \quad \text{and} \quad \varphi_2 = \omega_L \frac{L}{v_{2\perp}} = 2\pi c B L \frac{1}{k_{2\perp}}. \quad (4)$$

Here, the Larmor frequency $\omega_L = \gamma B$ with the neutron's gyromagnetic ratio $\gamma = 1.382 \cdot 10^8 \text{ s}^{-1} \text{ T}^{-1}$, $c = \gamma m / \hbar = 4.632 \cdot 10^{14} \text{ T}^{-1} \text{ m}^{-2}$, L is the length of the magnetic field perpendicular to the lattice planes, $k_{1\perp} = k_{2\perp} = k \sin \theta_0 = G_{hkl}/2$, and k is the neutron's wave number. The total precession is given by

$$\varphi_t = \varphi_1 + \varphi_2 = 2\pi cBL \left(\frac{1}{k_{1\perp}} + \frac{1}{k_{2\perp}} \right) = \frac{8\pi cBL}{G_{hkl}} = 4cBLd_{hkl}, \quad (5)$$

independent of the beam divergence $\Delta\theta$ or the neutron's wavelength λ . Note, that $\Delta\theta$ and λ are directly related through Bragg's law.

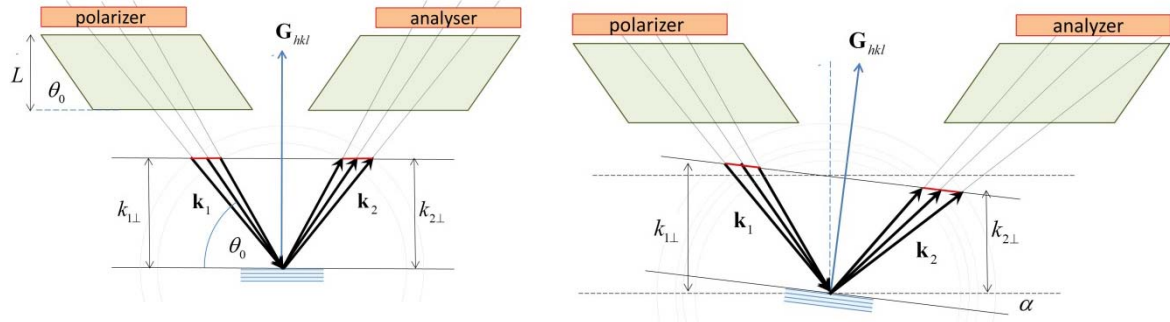


Figure 3. Schematic representation of a double-arm Larmor diffractometer. Left: single-crystal sample with lattice planes under investigation parallel to the faces of the precession regions. Right: misaligned single crystal.

If the crystal is misaligned with an angle α then $k_{1\perp}$ will be larger and $k_{2\perp}$ smaller, see Fig.3, resulting in cancellation of the effect of α in first order. This is shown mathematically as follows.

$$k_{1\perp} = k \sin(\theta_B + \alpha) \text{ and } k_{2\perp} = k \sin(\theta_B - \alpha). \quad (6)$$

Using the Bragg relation $k = G_{hkl} / (2 \sin \theta_B) = \pi / (d_{hkl} \sin \theta_B)$ and the Taylor expansion

$$1/\sin(\theta_B + \alpha) = 1/\sin \theta_B \left(1 - \cot \theta_B \alpha + 0.5(1 + 2 \cot^2 \theta_B) \alpha^2 + O(\alpha^3) \right) \text{ Eq.(5) reads to second order of } \alpha$$

$$\varphi_t = \varphi_1 + \varphi_2 = 4cBLd_{hkl} \left(1 + \frac{1}{2}(1 + 2 \cot^2 \theta_B) \alpha^2 \right). \quad (7)$$

The resolution in determining the lattice parameter d for this setup is given by

$$\left(\frac{\Delta d}{d} \right)^2 = \left(\frac{\Delta BL}{BL} \right)^2 + \frac{1}{4}(1 + 2 \cot^2 \theta_B)^2 \alpha^4. \quad (8)$$

If we now consider a *polycrystalline material*, or powder, all orientations of the lattice planes are present and the role of α in Eq.(8) is taken over by the beam divergence, resulting in a distribution of α with spread

$$\alpha^2 = \Delta\theta^2 + \Delta\phi^2, \quad (9)$$

where $\Delta\theta$ and $\Delta\phi$ are the divergences of the incoming and scattered beam, respectively. The intensity measured at the detector is given by $I(BL) = I_0(1 + P(BL))$ with I_0 the shim intensity and, if we only consider one Bragg peak,

$$P(BL) = \langle \cos \varphi_i \rangle = G(BL) \cos(4c \langle BL \rangle \langle d_{hkl} \rangle). \quad (10)$$

The period of the cosine determines the average lattice spacing and the damping envelope is given by $G(B) = \int f(\varphi - \varphi_0) \cos(\varphi) d\varphi$, where the distribution $f(\varphi)$ - see Eq.(7) - is determined by the distribution of the lattice spacing d_{hkl} , the field-integral aberrations, and angular uncertainties. In d_{hkl} -space these contributions are convolutions. This results in multiplying the Fourier transforms of these contributions in BL -space, leading to

$$G(BL) = G_{BL}(BL) G_\alpha(BL) G_d(BL). \quad (11)$$

G_d is the Fourier transform of the lattice-spacing distribution and G_{BL} and G_α describe the instrumental resolution. G_{BL} is determined by magnetic field B and its length L and can be measured by using a perfect single crystal as a calibration sample.

If more lattice parameters are measured simultaneously, The resulting intensity will be a sum of damped cosines with different periods and different damping. In Fig. 4 an example is shown of a perfect measurement, i.e. no beam divergence, no aberrations, i.e. $G_{BL} = G_\alpha = 1$ of a sample with two lattice parameters $d = 0.2$ and 0.5 nm, both normally distributed with a 0.5% standard deviation, corresponding with full width at half maximum of 1.9%. To the 1000 calculated intensities I , with spacing $\Delta BL = 1.36 \cdot 10^{-6}$ Tm, 10% statistics was added (corresponding with a shim intensity of 100 counts). Note, that the contribution of the 0.5 nm d -spacing is damped faster because of its larger width Δd . The resulting Fourier transform is shown in Fig.4. It shows that in this case 1000 measuring points with very modest statistics remarkably good lattice-parameter distribution functions can be reproduced. Note, that the oscillation of the background noise is an artefact of the Fourier transform.

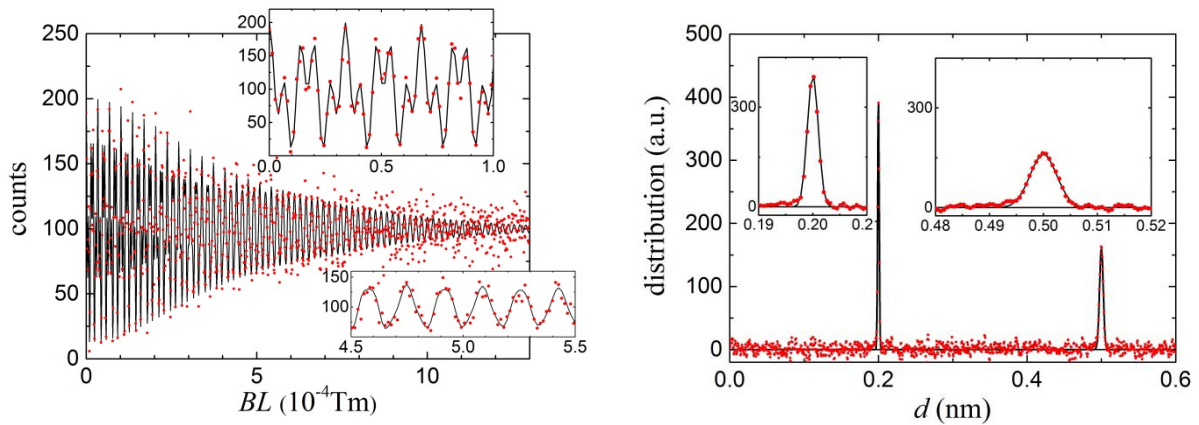


Figure 4. Simulation of a Larmor-diffraction experiment with perfect instrumental resolution. The model system has two lattice parameters d , each with a Gaussian distribution with 0.5% standard deviation (right, black line). Left: Fourier transform (black line) with 10% statistics added (red dots), representing experimental data. Note, that at the smaller BL values a beating representing both d values is present (inset top), while for larger BL mainly the contribution of $d = 0.2$ nm is present (inset bottom). The Fourier transform of the noisy data is displayed in the right panel (red dots).

4. Single-arm Larmor diffraction

4.1. Diffraction from perfect single crystal

If the sample is magnetic or has spin-flip scattering the double-arm setup may cause problems. Then the single-arm geometry, first described in [11], is a good alternative. In that case the analyzer is placed between the precession field and the sample, see Fig. 5. Whereas in the double-arm geometry the change of $k_{1\perp}$ as a result of the misalignment α is in first order compensated by the change of $k_{2\perp}$, see Fig. 3, this is not the case in the single-arm geometry, what will lead to a more modest resolution, as will be derived in the following. We will consider the single crystal and polycrystalline material separately.

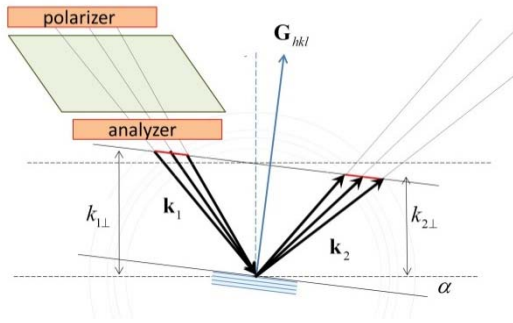


Figure 5. Schematic representation of a single-arm Larmor diffractometer with the Larmor precession device in the incoming beam. The angle α indicates the misalignment of the lattice planes with respect to the face of the precession region.

For a perfect single crystal, i.e. no mosaic spread, misaligned with angle α with respect to the face of the precession field, as indicated in Fig. 6, the Larmor precession phase is given by

$$\varphi_i = \varphi_1 = 2\pi cBL \frac{1}{k_{1\perp}} = 2cBLd_{hkl} \left(1 - \cot \theta_B \alpha + O(\alpha^2)\right). \quad (12)$$

This leads to a resolution that depends linearly on the spread in α :

$$\left(\frac{\Delta d}{d}\right)^2 = \left(\frac{\Delta BL}{BL}\right)^2 + \cot^2 \theta_B \Delta \alpha^2 \quad (13)$$

4.2. Powder diffraction

Whereas for the single-crystal case the small parameter is the misalignment α , for a polycrystalline sample the small parameters are the divergences of the incoming and the scattered beam. We define all angles with respect to the face of the precession field, see Fig.6.

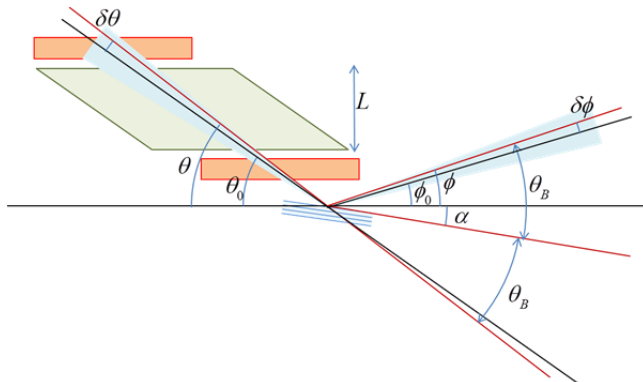


Figure 6. Schematic representation of a single-arm Larmor diffractometer with Larmor precession device in the incoming beam for the description of a powder sample. The nominal incoming and scattered beam (characterized by θ_0 and ϕ_0) are indicated by the black lines. A possible beam with deviations and are shown as red lines (characterized by θ and ϕ).

The nominal incoming angle is θ_0 . We follow the neutron path entering at incoming angle

$$\theta = \theta_0 + \delta\theta \quad (14)$$

and scattered at angle ϕ , determined by the nominal angle ϕ_0 and deviation $\delta\phi$

$$\phi = \phi_0 + \delta\phi. \quad (15)$$

The Bragg angle is given by

$$2\theta_B = \theta + \phi. \quad (16)$$

The relation between the actual Bragg angle θ_B and the nominal Bragg angle $\theta_{B0} = (\theta_0 + \phi_0)/2$ is given by $\theta_B = \theta_{B,0} + \delta\theta/2 + \delta\phi/2$. Note that the scattering-plane orientation $\alpha = \theta_B - \phi$ is not necessarily a small parameter. Using $k_{\perp} = k \sin \theta$ and $k = G_{hkl}/(2 \sin \theta_B) = \pi/(d_{hkl} \sin \theta_B)$, a Taylor expansion of $\varphi_1 = 2cBLd_{hkl} \sin \theta_B / \sin \theta = 2cBLd_{hkl} \sin(\theta_{B,0} + \delta\theta/2 + \delta\phi/2) / \sin(\theta_0 + \delta\theta)$ with small parameters $\delta\theta$ and $\delta\phi$ yields, in first order,

$$\varphi_1 = 2cBLd_{hkl} \frac{\sin \theta_{B,0}}{\sin \theta_0} \left[1 + (\cot \theta_{B,0} - 2 \cot \theta_0) \frac{\delta\theta}{2} + \cot \theta_{B,0} \frac{\delta\phi}{2} \right]. \quad (17)$$

If we assume $\delta\theta$ and $\delta\phi$ to be uncorrelated, which is the case for a polycrystalline sample, having distributions with spread $\Delta\theta$ and $\Delta\phi$, then this leads to the resolution

$$\left(\frac{\Delta d}{d} \right)^2 = \left(\frac{\Delta BL}{BL} \right)^2 + \frac{1}{4} (\cot \theta_{B,0} - 2 \cot \theta_0)^2 \Delta\theta^2 + \frac{1}{4} \cot^2 \theta_{B,0} \Delta\phi^2 \quad (18)$$

The contribution of the divergence of the incoming neutron beam to the resolution cancels in first order, if the focussing condition

$$\cot \theta_{B,0} = 2 \cot \theta_0 \quad (19)$$

is met, see Fig.7. It shows that by tuning the tilt angle the minimum resolution, that is of the order $\Delta d/d \approx 10^{-3}$ can be chosen to be at a scattering angle of choice.

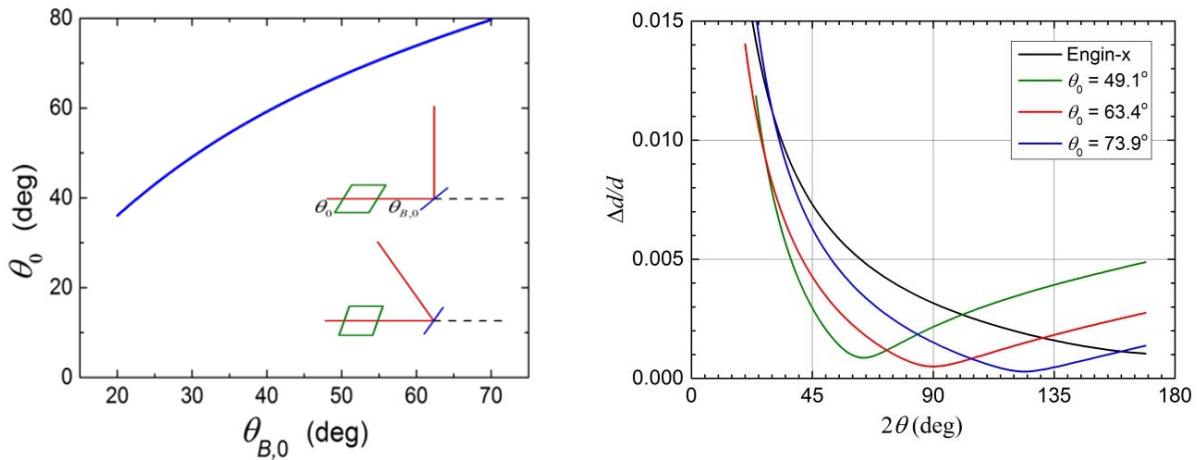


Figure 7. Left: Single-arm Larmor diffraction focusing condition, Eq.(19), for a polycrystalline sample. Right: resulting resolution for three different focusing conditions, corresponding $2\theta_B = 60^\circ$, 90° and 120° . Here the divergences of the incoming beam, $\Delta\theta$, and scattered beam, $\Delta\phi$, were taken 5

and 2 mrad, respectively. As a comparison the resolution of Engin-x is shown, with the same divergences.

4.3. Mosaic single crystal

For a powder the divergences $\delta\theta$ and $\delta\phi$ are uncorrelated, i.e. for any combination of divergences of incoming and scattered beam reflection planes are available. In the case of a mosaic crystal these parameters are correlated: assuming $\Delta\phi < \Delta\theta$, then for every value of $\delta\phi$ a range of $\delta\theta$ is available satisfying $\delta\theta = -\delta\phi + 2\delta\alpha$ for all $\delta\alpha$ within the mosaic spread $\Delta\alpha$. Then, for $\Delta\alpha < \Delta\theta$, Eq.(17) should be replaced by

$$\begin{aligned} \varphi_1 &= 2cBLd \frac{\sin\theta_{B,0}}{\sin\theta_0} \left[1 + (\cot\theta_{B,0} - 2\cot\theta_0) \frac{-\delta\phi + 2\delta\alpha}{2} + \cot\theta_{B,0} \frac{\delta\phi}{2} \right] \\ &= 2cBLd \frac{\sin\theta_{B,0}}{\sin\theta_0} \left[1 + (\cot\theta_{B,0} - 2\cot\theta_0)\delta\alpha + (\cot\theta_0 - \cot\theta_{B,0})\delta\phi \right], \end{aligned} \quad (20)$$

and then the resolution is given by

$$\left(\frac{\Delta d}{d} \right)^2 = \left(\frac{\Delta BL}{BL} \right)^2 + (\cot\theta_{B,0} - 2\cot\theta_0)^2 \Delta\alpha^2 + (\cot\theta_{B,0} - \cot\theta_0)^2 \Delta\phi^2. \quad (21)$$

In the double-arm geometry the mosaic spread only enters in second order, and is independent of the divergences of incoming and scattered beam, see Eq.(8). However, in the single-arm geometry the mosaic spread, in combination with the divergence $\Delta\phi$ of the scattered beam, will determine the resolution. Some examples are given in Fig. 8. For a perfect single crystal the minimum resolution is reached for scattering angle $2\theta_b = 2\theta_0$, conform Eq.(13). For increasing mosaic spread the minimum shifts to smaller scattering angles approaching the focusing value for powders, Eq.(19), if the mosaic spread approaches the divergence $\Delta\phi$ of the incoming beam.

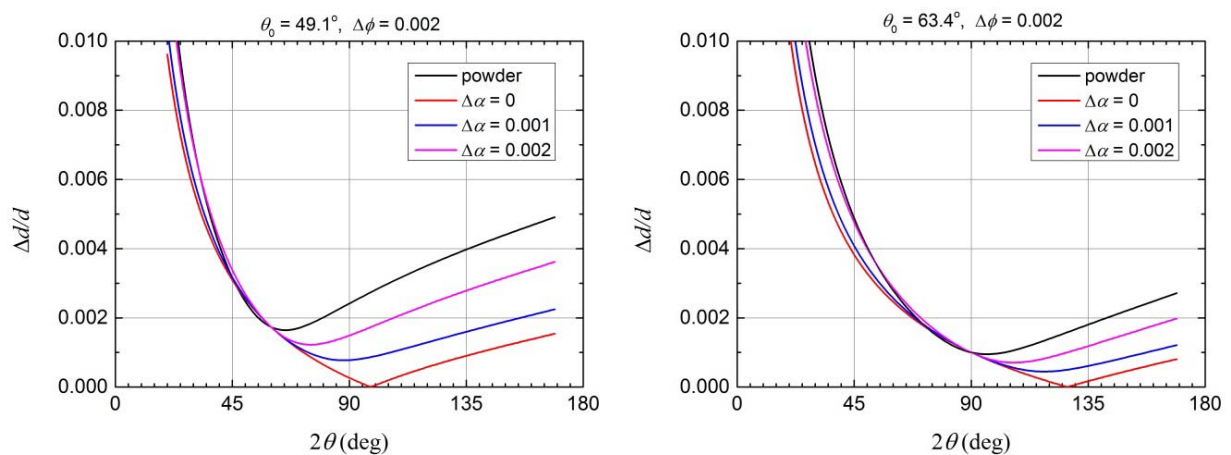


Figure 8. Resolution of a mosaic single crystal sample for three values of the mosaic spread $\Delta\alpha$ and two values of the precession-field tilt angle θ_0 . The divergence of the scattered beam is taken $\Delta\phi = 2$ mrad. As comparison, the resolution for a polycrystalline sample (with $\Delta\theta = 5$ mrad and $\Delta\phi = 2$ mrad) is shown (black line), also displayed in Fig. 7.

5. Discussion

Double-arm Larmor diffraction yields a resolution of $\Delta d/d \approx 10^{-6}$ that is orders of magnitude better than conventional diffractometers. For magnetic samples the single-arm geometry is a good alternative that may reach a resolution down to $\Delta d/d \approx 10^{-5}$ for single crystals and better than 10^{-3} for powder samples around the focussing condition, that can be set at any scattering at choice by changing the tilt angle of the precession region. For polycrystalline samples, the contribution of the divergence of the incoming beam is cancelled in first order at this focussing condition. This may be used to separate overlapping diffraction lines around this scattering angle while the data at the other scattering angles are used to increase the statistics. If the Larmor modulation is performed in the scattered beam instead of the incoming beam, a similar focussing condition will cancel the contribution of the divergence of the scattered beam.

One of the advantages of Larmor diffraction compared with monochromatic diffraction is the considerable gain in intensity because the former makes use of the total wavelength spectrum and accepts much larger beam divergences. Due to technical restrictions, the double-arm configuration has in general a limited range of scattering angles, while in the single-arm version a large range can be used. The argument that is often used against Larmor techniques that long measuring times are needed because one has to perform a large B scan is not valid. The important quantity is the total number of neutrons acquired. This is shown in Fig. 5 where the individual points have very poor statistics and the extracted information about the lattice-space distribution is of high quality. However, as a result of the Fourier technique the information in the tails of the distribution is less accurate.

A crucial part of Larmor diffraction is the accurate dimensioning of the precession fields. In practice this is established by using two radio-frequency neutron flippers per precession region. These have been implemented in the triple-axes spectrometers TRISP (FRM II, Munich) [20], FLEXX (HZB, Berlin) [21] and ZETA (ILL, Grenoble) [22]. These instruments are operated in a single wavelength mode, ideally suited for the investigation of a single Bragg peak. A general disadvantage of the Fourier technique is the fact that the contribution of low-intensity Bragg peaks is difficult to detect in the measured data, that are mainly determined by the high-intensity peaks. For this reason Larmor diffraction is especially suited for determining the intensity and shape of a limited number of Bragg peaks, e.g. for strain scanning. Usually this technique is used at a scattering angle of 90 degrees. Fig.7. shows that at that angle Larmor diffraction is considerably better than Engin-x, ISIS. The Fourier technique is also applied by making use of a Fourier chopper, examples being FSS at the former GKSS, Geesthacht [24] and FSD, IBR-2, Dubna [25]. The advantage of the Larmor diffraction is that there are no rotating parts and that a many orders in Fourier space can be covered electronically.

The comparison of applying the technique at a steady-state (reactor) and a pulsed (spallation) source is not straight forward. If only one Bragg peak is investigated the reactor sources are better compared to the present spallation sources. Because the sample acts as a monochromator the neutron intensity will be considerably higher in the former. If the Larmor diffractometer makes use of the complete spectrum it is in principle possible to measure more Bragg peaks simultaneously, as shown in ref [11]. However, in that case it will be difficult to measure low-intensity peaks. This problem can be circumvented at a pulsed source. Then the different time-of-flight channels will only contain a few Bragg peaks, even at relaxed time-of-flight resolution. The ESS, Lund, will be the ideal source for the Larmor diffraction technique. It combines a high average neutron flux, comparable with ILL, with a sufficient time-of-flight resolution. Having a broad-wavelength spectrum makes it possible to measure many Bragg peaks at one scattering angle in focussing condition. Possible application may be found in multiple-phase systems where precise d spacing and distribution for all phases can be determined; for separating two overlapping Bragg peaks; in engineering materials determining Q -dependent line broadening to discriminate grain-size and micro-strain contributions; the information from more lattice planes will give information about anisotropic strain.

References

- [1] C. Pfleiderer, P. Böni, T. Keller, U.K. Rößler, A. Rosch, *Science* **316** (2007) 1871
- [2] N. Martin, L.P. Regnault, S. Klimko, *J. Phys: Conf. Series* **340** (2012) 012012
- [3] J. Repper, T. Keller, M. Hofmann, C. Krempaszky, W. Petry, E. Werner, *Acta Materialia* **58** (2010) 3459
- [4] I. Lucks, P. Lamparter, E. J. Mittemeijer, *J. Appl. Cryst.* **37** (2004) 300
- [5] T.C. Bor, H.H.M. Cleveringa, R. Delhez, E. van der Giessen, *Mater. Sci. Engin.* **A309–310** (2001) 505
- [6] F. Mezei, *Zeitschrift für Physik A* **255** (1972) 146
- [7] R. Pynn, in *Neutron Spin Echo*, ed. F. Mezei, Springer-Verlag, Berlin, 1980
- [8] T. Keller, R. Gähler, H. Kunze, R. Golub, *Neutron News* **6** (1995); M.T. Rekveldt, *Nucl. Instr. Meth. Phys. Res. B* **114** (1996) 366
- [9] M.T. Rekveldt, *Physica B* **234-236** (1997) 1135
- [10] M.T. Rekveldt, W.H. Kraan, *J. Neutron Res.* **8** (1999); M.T. Rekveldt, T. Keller, R. Golub, *Europhys. Lett.* **54** (2001) 342
- [11] M.T. Rekveldt, J. Plomp, A.A. van Well, *J. Appl. Cryst.* **47** (2014) 436
- [12] G. Caglioti, A. Paoletti, F.P. Ricci, *Nucl. Instr.* **3** (1958) 223
- [13] A.W. Hewat, *Nucl. Instr. Meth.* **127** (1975) 361
- [14] T.C. Hansen et al., *Meas. Sci. Technol.* **19** (2008) 034001
- [15] M. Hoelzel, A. Senyshyn, N. Juenke, H. Boysen, W. Schmahl, H. Fuess, *Nucl. Instr. Meth. A* **667** (2012) 32
- [16] http://www-llb.cea.fr/en/Web/hpr_web/HPRWEB5.php
- [17] C.G. Windsor, *Pulsed Neutron Scattering*, (1981) London: Taylor and Francis.
- [18] R.M. Ibberson, *Nucl. Instr. Meth. A* **600** (2009) 47
- [19] J. R. Santisteban, M.R. Daymond, J.A. Jamesb, L. Edwards, *J. Appl. Cryst.* **39** (2006) 812
- [20] T. Keller, B. Keimer, *J. Large-scale Res. Fac. A* **37** (2015) 1
- [21] F. Groitl, T. Keller, D.L. Quintero-Castro, K. Habicht, *Rev. Sci. Instr.* **86** (2015) 025110
- [22] N. Martin, L.P. Regnault, S. Klimko, J.E. Lorenzo, R. Gähler, *Physica B* **406** (2011) 2333
- [23] H. Pöyry, P. Hiismäki, Virjo, *Nucl. Instr. Meth.* **126** (1975) 421
- [24] J. Schröder, V.A. Kudryashev, J.M. Keuter, H.G. Priesmeyer, J. Larsen, A. Tiitta, *J. Neutron Res.* **4** (1994) 129; V.A. Kudryashev, H.G. Priesmaeyer, J.M. Keuter, J. Schröder, R. Wagner, *Nucl. Instr. Meth. Phys. Res. B* **101** (1995) 484
- [25] A.M. Balagurov, G.D. Bokuchava, E.S. Kuzmin, A.V. Tamonov, V.V. Zhuk, *Z. Kristallogr. Suppl.* **23** (2006) 217; A.M. Balagurov, I.A. Bobrilov, G.D. Bokuchava, V.V. Zhuravlev, V.G. Simkin, *Phys. Part. Nucl.* **46** (2015) 249

Appendix: Double-arm spin-echo geometry

In the spin-echo geometry the direction of the magnetic field in the second arm is opposite to that of the first arm. The total precession angle for a perfect single crystal with misalignment angle α is

$$\varphi_t = \varphi_1 - \varphi_2 = 4cBLd_{hkl} \left(-\cot \theta_B \alpha + O(\alpha^3) \right). \quad (\text{A1})$$

and

$$P(BL) = G(BL) = \int f(\varphi) \cos(\varphi) d\varphi \quad (1)$$

where the distribution $f(\varphi)$ is determined by both the spreads in lattice spacing d_{hkl} and the misalignment parameter α .

$$\left(\frac{\Delta\varphi}{\varphi} \right)^2 = \left(\frac{\Delta BL}{BL} \right)^2 + \left(\frac{\Delta d_{hkl}}{d_{hkl}} \right)^2 + (\Delta\alpha)^2 \quad (\text{A2})$$

For a *single crystal* sample the variation in lattice parameter may be neglected and $P(BL)$ directly yields the mosaic spread. For a *polycrystalline* sample $P(BL)$ yields the distribution of the lattice parameter, i.e. the Fourier transform of the Bragg peak. In ref [7] it is stated that in this setup the peak shape can be determined with ‘extremely fine’ resolution. However, we show that for a polycrystalline sample the peak is broadened by the angular resolution of the setup. Here, the same arguments hold as for the parallel-field geometry.